

## Statistical Analysis of Highly Unsteady Phenomena in Transonic Flow (Part I: Analysis in The Frequency Domain)

A. Al Shabu

Mechanical Engineering Department/ College of Engineering Technology Janzour,  
Tripoli, Libya

### Abstract

The current paper introduces the first part of a comprehensive statistical analysis of a highly unsteady phenomena observed in the transonic flow on a BAC3-11 airfoil model with a constant chord length and a sharp trailing edge. The investigations are performed in a modified shock tube with a rectangular test section. In addition to time-resolved shadowgraphs pressure histories measured on the suction side of the model reveal clearly the existence of pressure waves initiated near the trailing edge and propagating upstream where they become apparently weaker near the leading edge. In a first step the obtained pressure histories are analyzed in the frequency domain (Fourier-analysis). The power spectra of these fluctuations reveal dominant frequencies about 1 kHz, 1.5 kHz and 2.3 kHz. The periodical part of the captured fluctuations is also revealed by the autocorrelation function. However, the non-periodical part of the signals cannot be quantified using the classical autocorrelation function. Using the two-point cross correlation, the wave speed, absolute wave Mach number and the wave propagation direction are determined. The determined wave Mach number is slightly above 1, which means that the observed waves represent weak shocks propagating slightly faster than the speed of sound. However, the merit of the signal analysis in the frequency domain is limited when analysing phenomena of high degree of unsteadiness like the one being investigated. A more powerful and suitable tool for the analysis of the observed waves in the time-frequency domain will be addressed in a following paper.

**Keywords:** Shock tube, transonic flow, upstream moving waves, Fourier analysis, autocorrelation, cross correlation.

### 1. Introduction

In [1] an interesting experimentally observed phenomenon in the transonic flow on an airfoil was presented. This phenomenon can be described in terms of pressure waves build up near the trailing edge and / or in the wake and propagate upstream, where they interact with the incoming flow, strengthen before becoming apparently weaker and almost disappear near the leading edge. Both experimental and numerical investigations showed that the propagation of the observed waves is coupled with vortex generation in the boundary layer and wake fluctuations [1], [2], [3]. As discussed in [1] the phenomenon of upstream moving pressure waves had already been observed by several authors upon investigating the phenomenon of periodic shock motions on airfoils. It was, however, pointed out that the investigated upstream moving waves had been observed for flow conditions for which no shock or shock oscillations had occurred. The vortex generation in the boundary layer as well as the interaction of vortices with the trailing edge play apparently a key role in the generation of these waves [4], [5], [6], [7], [8]. Based on the preliminary analysis of the observed waves presented in [1] a more comprehensive statistical analysis has been done to extract as much information from the experimental data as possible which allows for better understanding of the observed waves. This is done in the frequency domain (Fourier-Analysis) as well as in the frequency-time domain (Wavelet-Analysis). This

paper presents the first part of the statistical analysis, i.e. analysis in the frequency domain (Fourier-Analysis).

### 2. Theoretical Background

Experimental data are digital time series mainly pressure histories. To analyze these large sets of data, well established signal processing methods are used to extract as much information from experimental data as possible. In the following useful tools for signal analysis in the frequency domain (Fourier Analysis), used in this paper, will be discussed.

#### 2.1 Fourier Transform

The Fourier transform identifies the different frequency sinusoids in a signal and their respective amplitudes, i.e. it is simply a frequency-domain representation (frequency content) of a signal. For one dimensional signal  $x(t)$  the Fourier transform is defined as [9]:

$$X(i2\pi f) = \int_{-\infty}^{\infty} x(t)e^{-i2\pi ft} dt \quad (1)$$

For a digital signal  $x_k$  sampled at discrete time intervals  $\Delta T$  within a total measurement time  $T$  the discrete Fourier transform (DFT) is used instead. This is defined as [10]:

$$\text{DFT}(x_n) = \frac{1}{N} \sum_{k=0}^{N-1} x_k e^{-i2\pi f_n k \Delta T} \quad (2)$$

where  $N = T/\Delta T$  is the number of samples, and  $f_n = n/T$ ;  $n = 0, 1, 2, \dots, N-1$  are the discrete frequency components.

In the practice and in order to drastically reduce calculation time, an algorithm called Fast Fourier Transform (FFT) is used to compute the Discrete Fourier Transform DFT. For more details please refer to [9], [10], [11].

## 2.2 Standard deviation

The standard deviation is the positive root of the variance, which is the second central moment of a distribution. It is a measure of the dispersion of the measured values with respect the mean value  $\bar{x}$  [9]. The standard deviation for discrete-time signals is given by:

$$\sigma = \sqrt{\frac{1}{N} \sum_{n=1}^N (x_n - \bar{x})^2} \quad (3)$$

The normalized standard deviation of the pressure signals by the static pressure of the incoming flow can be used as a measure of the intensity of the fluctuations over the airfoil chord (section 4).

## 2.3 Autocorrelation function (ACF)

Using the autocorrelation function, it is possible to separate periodical from nonperiodical parts of a signal. This allows for detecting the self similarity of the signal being investigated. The auto correlation function is given by Eq. (4) [9]

$$\Phi_{xx}(\tau) = \lim_{T \rightarrow \infty} \frac{1}{x_{eff}^2} \frac{1}{2T} \int_{-T}^T x(t)x(t-\tau) dt \quad (4)$$

where  $\tau$  is a specified time shift and  $x_{eff}$  is a normalization factor and it corresponds to the auto-correlation value for zero time shift  $\tau$  (full matching)

$$x_{eff}^2 = \Phi_{xx}(\tau = 0) = \lim_{T \rightarrow \infty} \frac{1}{2T} \int_{-T}^T x^2(t) dt \quad (5)$$

For a given signal  $x(t)$  consisting of superposition of other signals the ACF of  $x(t)$  is the sum of the ACF's of the signals consisting it. For digital time series an adequate formula [10], [11] is used for numerical computation of the ACF given by Eq. (6)

$$\Phi_{xx}(k\Delta T) = \frac{1}{x_{eff}^2} \frac{1}{N} \sum_{n=0}^{N-1} x(n\Delta T)x([n-k]\Delta T); \quad k = 0, 1, 2, 3, \dots \quad (6)$$

where  $N$  is the number of sampling points and  $\Delta T$  is the sampling period.

## 2.4 Cross correlation function (CCF)

Analogous to the autocorrelation function the cross correlation function is a measure of the eventually existing similarity of two signals  $x(t)$  and  $y(t)$  Eq. () [9]

$$\Phi_{xy}(\tau) = \lim_{T \rightarrow \infty} \frac{1}{x_{eff} y_{eff}} \frac{1}{2T} \int_{-T}^T x(t)y(t-\tau) dt \quad (7)$$

where  $x_{eff}$  and  $y_{eff}$  are normalization factors (compare Eq. (5)). For correlated signals the CCF allows for the separation of periodical signals from stochastic noise. One of the advantages of the CCF is its use for determination of a wave speed when this wave is sensed at two different locations (Two-Point cross correlation). The travelling time for such wave, corresponding to the time shift of the maximum matching, can be determined. This calculated speed must be understood though as an overall average speed of all frequencies – or at least the dominant ones – contained in the signal or wave. Similarly, Eq. (8) gives an adequate formula for digital computation of the CCF [10], [11]:

$$\Phi_{xy}(k\Delta T) = \frac{1}{x_{eff} y_{eff}} \frac{1}{N} \sum_{n=0}^{N-1} x(n\Delta T)y([n-k]\Delta T); \quad k = 0, 1, 2, 3, \dots \quad (8)$$

where  $N$  is again the number of sampling points and  $\Delta T$  is the sampling period.

### 2.5 Absolute wave speed

The absolute wave speed or the speed with respect to the local flow  $u^*$  is obtained when the local flow speed  $u_{loc}$  is added to the speed determined by the cross correlation  $u_w$  as given by Eq. (9)

$$u^* = u_w + u_{loc} \quad (9)$$

Assuming one-dimensional isentropic flow, the local flow speed can be expressed as:

$$u_{loc} = u_\infty \sqrt{\left[1 - \frac{2}{(\gamma - 1)Ma_\infty^2} \left( \left( \frac{\gamma}{2} Ma_\infty^2 cp + 1 \right)^{\frac{\gamma-1}{\gamma}} - 1 \right)\right]} \quad (10)$$

where  $u_\infty$  is the free stream flow velocity which can be determined using the shock tube relations.  $cp$  is the pressure coefficient at the corresponding sensor position given by:

$$cp = \frac{2}{\gamma Ma_\infty^2} \left( \frac{p}{p_\infty} - 1 \right) \quad (11)$$

where  $p_\infty$  and  $p$  are the free stream and the local static pressure respectively.

The absolute wave Mach number  $Ma^*$  can be obtained when Eq. (9) is divided by the local sound speed  $a_{loc}$

$$\frac{u^*}{a_{loc}} = \frac{u_w}{a_{loc}} + \frac{u_{loc}}{a_{loc}} \quad (12)$$

$$Ma^* = \frac{u_w}{a_{loc}} + Ma_{loc} \quad (13)$$

where  $Ma_{loc}$  is the local flow Mach number given by:

$$Ma_{loc} = \sqrt{\frac{1}{\gamma - 1} \left[ 2 + (\gamma - 1) Ma_\infty^2 \left( \left( \frac{\gamma}{2} Ma_\infty^2 cp + 1 \right)^{\frac{\gamma-1}{\gamma}} - 2 \right) \right]} \quad (14)$$

with

$$a_{loc} = \frac{u_{loc}}{Ma_{loc}} \quad (15)$$

### 3. Experimental

The test facility used is a modified shock tube with a rectangular test section (280 x 200 mm) to perform airfoil testing at transonic Mach numbers and relatively high Reynolds numbers extending up to  $38 \times 10^6$  based on a chord length of 100 mm. The flow behind the incident shock wave provides the testing flow for a measurement period of about 5 ms. The facility and its wave plan are depicted in Fig. 1. A full description of the facility and its working principle can be found in [12]. The tested model is BAC3-11 airfoil with 200-mm span, 80-mm chord length and a sharp trailing edge. To perform pressure measurements, 11 pressure transducers of the commercial Kulite XCQ-080 are mounted directly beneath pressure taps of 0.6-mm diameter to minimize the influence of the pressure transmitting volume on the pressure signals (Fig. 2). The enclosed volume  $V$  between sensor membrane and pressure tap is  $3.45 \text{ mm}^3$ . The natural frequency of the Helmholtz resonator [13], [14] of the resulting configuration consisting of pressure tap, transmitting volume and sensor is about 6 kHz. The chord positions of the pressure taps are given in Table 1.

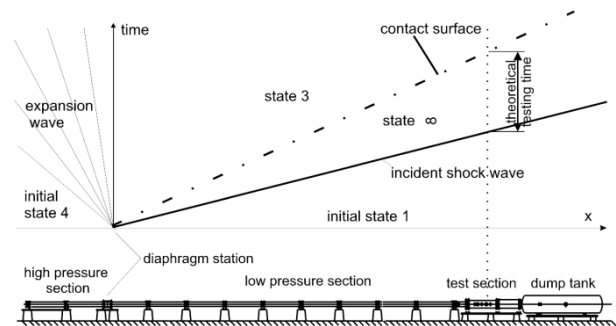


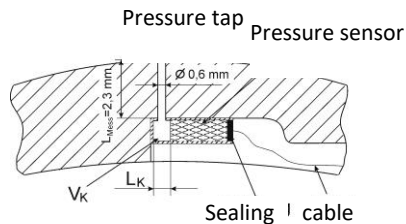
Fig. 1 Schematic of Transonic Shock Tube and its wave plan [1].

Table 1: Chord positions of the pressure taps

|          |     |     |     |     |     |     |     |
|----------|-----|-----|-----|-----|-----|-----|-----|
| Sensor   | 1   | 2   | 3   | 4   | 5   | 6   | 7   |
| Position | 0.1 | 0.1 | 0.2 | 0.3 | 0.3 | 0.4 | 0.4 |
| x/c      | 1   | 8   | 5   | 1   | 7   | 3   | 9   |
| Sensor   | 8   | 9   | 10  | 11  |     |     |     |
| Position | 0.5 | 0.6 | 0.6 | 0.7 |     |     |     |
| x/c      | 5   | 1   | 7   | 3   |     |     |     |

The airfoil model is fixed to the two tunnel side walls by two thin side plates with a thickness of 3 mm. Therefore, either the suction or pressure side of the airfoil and the corresponding flow field is visible. Fig. 3 shows a typical example of a pitot and static pressure history measured in the test section. Due to shock-tube boundary layer effects, both pressures slightly increase with time. For analyzing data a time window is chosen between 8 and 12 ms, during which the free stream Mach number changes only by 1.4 %. The maximum uncertainty in the measurements is as follows:  $p = \pm 3\%$ ,  $Ma = \pm 4.7\%$ ,  $Re = \pm 5.8\%$ , and  $u = \pm 4.5\%$ .

For flow visualization, high-speed photography is used to obtain highly time-resolved shadowgraphs and schlieren pictures of the flow [1].



**Fig. 2 Pressure measurement configuration (schematic)**  
[1]

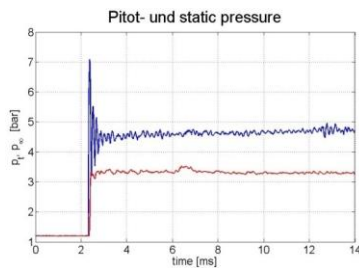
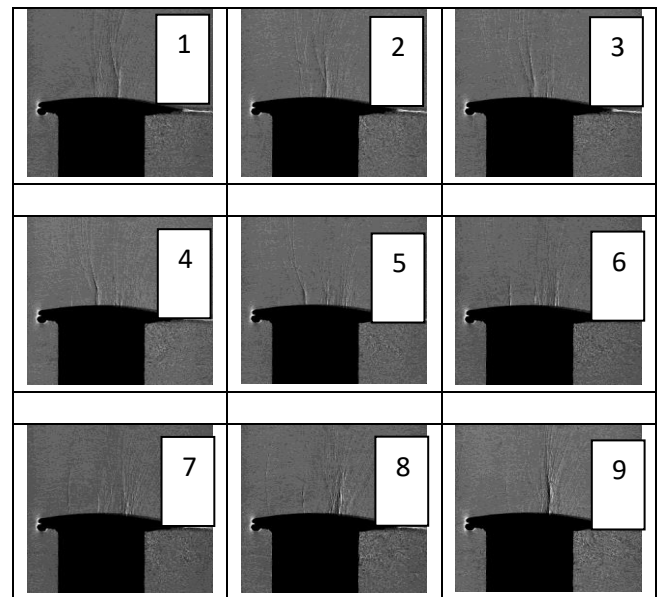


**Fig. 3 Pitot and static pressure histories measured in the test section of the transonic shock tube**

#### 4. Results

For the following discussion an experiment at a Mach number of 0.71 and a Reynolds number of  $2.0 \times 10^6$  has been chosen. Fig. 4 shows the corresponding time-resolved shadowgraphs for this experiment. The wave structure on the suction side of the airfoil and the upstream propagation of the waves can be easily seen. An increase in the wave intensity is also seen in the region of maximum thickness of the airfoil. The intensity of the waves decreases, however, as they move further upstream toward the leading edge. Here, they become almost invisible, depending on the

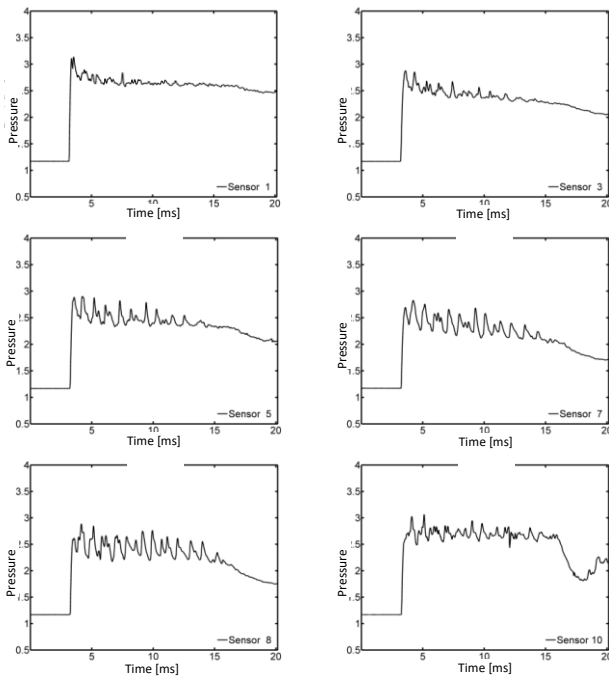
sensitivity of the shadowgraph system. Because of the line-of-sight effect of the shadowgraphs and the limited sensitivity of the optical system, it is difficult to identify vortex structures in the shadowgraphs. However, numerical simulations [8] confirm that the wave generation is coupled with vortex generation in the boundary layer. These vortices propagate downstream and interact with the trailing edge and/or the wake, causing the waves to initiate [1], [8]. Parallel to flow visualization, pressure measurements on the suction side of the BAC3-11 airfoil were also performed. Fig. 5 shows some selected pressure histories for the above experiment. Pressure fluctuations in the pressure histories resulting from the aforementioned wave processes can be seen. Starting from the trailing edge, the intensity of these fluctuations increases in the region of maximum thickness of the airfoil before decreasing strongly near the leading edge. This confirms the conclusion made from the shadowgraphs. As described next, these fluctuations were analyzed by statistical means.



**Fig. 4 Time-resolved shadowgraphs showing the wave propagation on the suction side of the BAC3-11;  $Ma = 0.71$ ,  $Re = 2.0 \times 10^6$ ,  $\alpha = 0$  deg, and  $\Delta t = 0.114$  ms.**

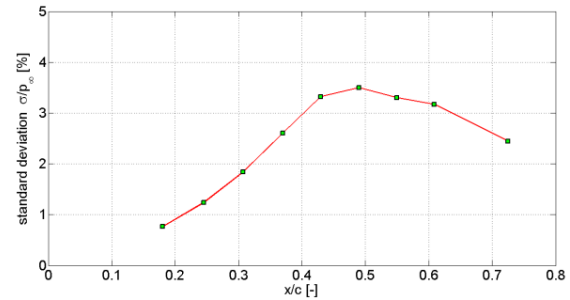
Figure 6 shows the standard deviation of the obtained pressure signals for the time interval from 8 to 12 ms, normalized with the free-stream static pressure  $p_\infty$ . The standard deviation, which can be regarded as a measure of the wave intensity, confirms the preceding conclusion. Starting with pressure fluctuations of about 2.5% at the chord position  $x/c = 0.73$ , the pressure fluctuations intensify upstream, reaching a maximum of about 3.5% at  $x/c = 0.49$  before decreasing rapidly further upstream to less than 1.0%

at  $x/c = 0.18$ . In Fig. 7 the autocorrelation functions are exemplary shown for the pressure histories at the chord positions  $x/c = 0.37$  and  $0.73$ . The repeated peaks of the autocorrelation functions indicate the periodical nature of the wave processes, and the two neighbouring peaks indicate the existence of two predominant frequencies represented in the signal. The envelopes (dashed lines) in Fig. 7 correspond to the autocorrelation values of a pure sinusoidal signal. The difference between the autocorrelation values and these envelopes clearly indicate the existence of non-periodical part in the pressure signals which cannot be further investigated by the classical autocorrelation. Figure 8 shows the power spectral density of the same pressure histories presented in Fig. 7. Figure 8 reveals two predominant frequencies ranging from 0.7 to 1.5 kHz and a relatively weaker one around 2.3 kHz. The same holds for other pressure histories.

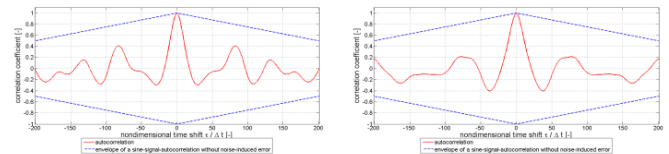


**Fig. 5 Pressure histories corresponding to the wave propagation on the suction side of the BAC3-11;  $Ma = 0.71$ ,  $Re = 2.0 \times 10^6$ ,  $\alpha = 0 \text{ deg}$**

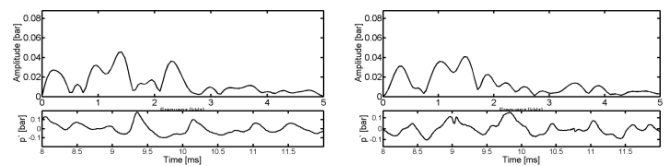
As already mentioned in section 2.4 the averaged wave speed between the sensors is estimated by knowing the distance between the sensors. Figure 9 shows exemplary the cross correlation for sensor 5 ( $x/c = 0.37$ , left) and sensor 11 ( $x/c = 0.73$ , right) and the estimated wave speed at the corresponding position. The negative time delays of the correlation function of the pressure sensors located upstream of the considered position ( $x/c = 0.73$ ) indicate that the pressure waves propagate upstream, Fig. 9 (right).



**Fig. 6 Normalized standard deviation of the pressure histories shown in Fig. 5**

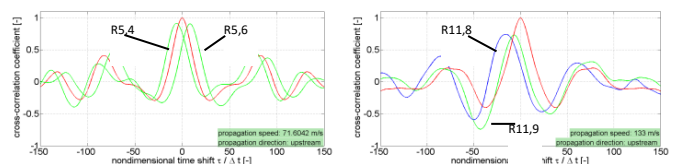


**Fig. 7 Autocorrelation functions for the pressure histories at the chord positions  $x/c = 0.37$  and  $0.73$**

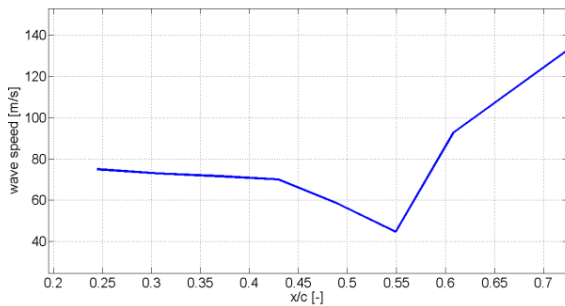


**Fig. 8 Power spectrum for the pressure histories shown in Fig. 7**

Depending on the relative position of the two sensors being correlated, positive or negative time delays result, as shown in Fig. 9 (left). It should be mentioned that the fluctuations at sensors 1 and 2 are so weak that no reasonable results could be obtained from the cross-correlation. Therefore, the estimation of the wave speed is only possible between sensor 3 and sensor 11.



**Fig. 9 Cross correlation function at sensor 5 (left) and sensor 10 (right) with some selected pressure gauges located up- and downstream**



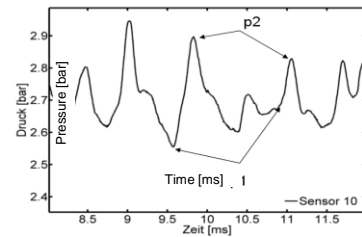
**Fig. 10 Estimated wave speed along BAC3-11 airfoil suction side using the classical cross-correlation**

Figure 10 shows the wave speed relative to the airfoil. Regardless of the rough spatial resolution, the figure displays the expected behavior of the wave speed. It can be easily seen that the wave speed is lowest in the region of high local flow velocities and increases further down-stream in the recompression zone of the airfoil. In Fig. 11 the curves of the relative wave speed (top left), the local flow speed (top right), the absolute wave velocity (bottom left) and the absolute wave Mach number (bottom right) along the airfoil chord are depicted (compare section 2.5). The discontinuous curves are due to the limited number of sensor positions. It is remarkable in Fig. 11, that the maximum of the local flow speed and the minimum of the wave speed, determined by the cross-correlation, does not exactly occur at the same location. The minimal wave speed is thus somewhat downstream of the pressure minimum. Furthermore, the curve of the wave Mach number reveals a maximum in the range of the maximum displacement of the airfoil  $x/c = 0.40$  to  $0.55$ . There it reaches a value of 1.17. In the rear and front airfoil part the wave Mach number lays around the value 1.13. The wave Mach number can also be estimated by the following relationship:

$$Ma_{wave} = \sqrt{\frac{(\gamma+1)p_{21} + \gamma - 1}{2\gamma}} \quad (16)$$

Eq. (16) is based on one-dimensional consideration of the Mach number of moving wave in a gas at rest. The pressure ratio over the waves is given by  $p_{21} = p_2 / p_1$ , as shown in Fig. 12 exemplary for the pressure history of the sensor 10 ( $x/c = 0.67$ ). Since all pressure histories reveal an amplitude spectrum and thus for simplicity, Eq. (16) is evaluated only for the maximum and minimum pressure ratio of the respective pressure history, resulting in a maximum and minimum wave Mach number at the respective sensor position.

Depicted in Fig. 13 are the so determined wave Mach numbers in addition to the average wave Mach number over airfoil chord. For comparison, the curve of the wave Mach number determined based on the cross correlation is also shown in Fig. 13. Along the airfoil chord the curve of the cross correlation wave Mach number lays clearly above the average wave Mach number estimated by Eq. (16). The deviations reach up to 9%. However, the maximum of the wave Mach number in the two curves occurs at the same position ( $x/c = 0.49$ ). Concerning the above comparison following points must be noted :



**Fig. 11 Pressure history of sensor 10**

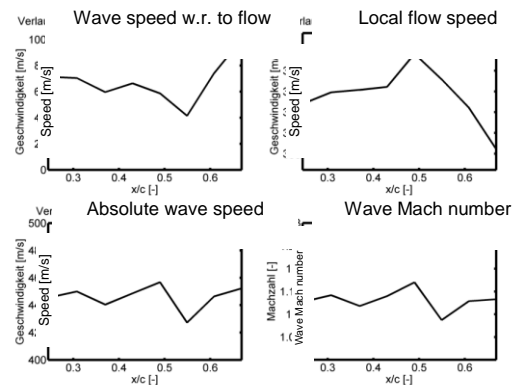


**Fig. 12 Absolute and relative wave speeds, flow speed and absolute wave Mach number along the airfoil**

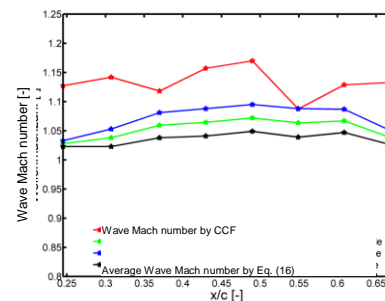


**Fig. 26 Comparison of the wave Mach numbers along the airfoil**

- Observed here is a complicated phenomenon by which relatively weak waves emanating at the trailing edge of an airfoil, propagate upstream at higher speed and interact with the flow pattern established. In the chord area around  $x/c = 0.55$  these waves decelerate, coalesce and form a shock, whose stability depends on the flow regime and thus on the free stream conditions [1].
- For lower free stream Mach numbers as the one shown in the investigated example the formed shock is not stable and immediately degenerate into compression waves which keep propagating upstream. For higher Mach numbers a large supersonic region terminated by shock forms and a strong wave-shock interaction takes place, by which weaker pseudo upstream moving waves form in the supersonic [1].
- Equation (16) describes the propagation of waves in a gas at rest and does not assess the complexity of the phenomenon described above and hence might not be fully applicable here.
- Finally, the above discussion makes very clear that the spatial resolution of the pressure histories in the chord region  $x/c = 0.49$  -  $x/c = 0.60$  is not sufficient and needs to be improved. Increasing the spatial resolution will also result in more accurate wave speed determined by the cross-correlation.

## 5. Conclusion

Transonic flow investigations are performed in a modified shock tube with a rectangular test section. The investigated model is a BAC3-11 airfoil with a constant chord length and a sharp trailing edge. Time-resolved shadowgraphs and schlieren pictures show pressure waves initiated near the trailing edge and propagating upstream where they become apparently weaker near the leading edge. The observed waves are also captured by pressure transducers mounted in the airfoil model. The power spectra of these fluctuations reveal dominant frequencies about 1 kHz, 1.5 kHz and 2.3 kHz. The periodical part of the captured fluctuations is also revealed by the autocorrelation function. However, a comparison with the envelopes of autocorrelation of a periodical (sinusoidal) function clearly indicates the existence of non-periodical part in the fluctuations caused by unsteadiness of the observed phenomena. This non-periodical part cannot be quantified using the statistical autocorrelation function. Using two-point cross correlation, the wave speed with respect to airfoil and wave propagation direction are determined. With the local flow speed the absolute wave speed, i.e. with respect to flow and absolute wave Mach number are also determined. As expected, the wave Mach number is slightly above 1, which means that with respect to flow the observed waves can be described as weak shock waves propagate slightly faster than the speed of sound. In general, it can be concluded that the merit of

the signal analysis in the frequency domain is limited when analysing a phenomenon of high degree of unsteadiness like the one being investigated. A more powerful and suitable tool for the analysis is the wavelet analysis, which gives a time-frequency representation of the signal. More information can be extracted from the signals. This will be addressed in a following paper.

## Nomenclature:

|                        |   |  |
|------------------------|---|--|
| $a_{\infty}$           | = | sound speed at free stream conditions                    |
| $c$                    | = | airfoil chord  |
| $Ma$                   | = | Mach number  |
| $Ma_{\infty}$          | = | free stream Mach number                                  |
| $p$                    | = | static pressure  |
| $p_t$                  | = | stagnation or pitot pressure                             |
| $\phi_{xx}, \phi_{xy}$ | = | auto- or cross correlation                               |
| $R_e$                  | = | Reynolds number  |
| $T_0$                  | = | stagnation temperature                                   |
| $u$                    | = | velocity   |
| $u_{\infty}$           | = | free stream flow velocity                                |
| $u_{loc}$              | = | local flow velocity                                      |
| $u_w$                  | = | wave speed relative to the airfoil                       |
| $u^*$                  | = | wave speed relative to the flow                          |
| $V$                    | = | enclosed volume between pressure sensor and pressure tap |
| $\alpha$               | = | angle of attack  |
| $\gamma$               | = | ratio of specific heats                                  |
| $\tau$                 | = | time delay, time shift parameter                         |
| $x(t)$                 | = | continuous signal  |
| $X(i2\pi f)$           | = | Fourier Transform of a signal $x(t)$                     |
| DFT                    | = | Discrete Fourier Transform                               |
| $x_n, x_k$             | = | sample of index $n$ or $k$                               |
| $N$                    | = | number of samples of a digital time series               |
| $f$                    | = | frequency in Hz  |
| $T$                    | = | signal period  |
| $\Delta T$             | = | sampling period  |
| $x_{eff}, y_{eff}$     | = | normalization factors for auto- and cross correlation    |
| ACF                    | = | Autocorrelation Function                                 |
| CCF                    | = | Cross Correlation Function                               |
| $\Delta\tau$           | = | change of the shift parameter                            |

### Acknowledgments

The author would like to thank the German Research Association DFG (Deutsche Forschungsgemeinschaft) for their financial support of this work.

### References

1. Alshabu, A. and Olivier, H., "Unsteady Wave Phenomena on a Supercritical Airfoil", AIAA Journal, Vol. 46, No. 8, pp. 2066-2073, August 2008. DOI: 10.2514/1.35516.
2. Alshabu, A., Olivier, H., and Klioutchnikov, I., "Investigation of Upstream moving Pressure Waves on a Supercritical Airfoil", Aerospace Science and Technology, Vol. 10, pp. 465-473, May 2006. DOI: 10.1016/j.ast.2006.04.003.
3. Klioutchnikov I., Ballmann J.: DNS of transitional transonic flow about a supercritical BAC3-11 airfoil using high-order shock capturing schemes. DLES VI, Springer-Verlag, ERCOFTAC Series, Vol. 126, No. 1, pp. 737-744, 2006.
4. Gibb J.: "The cause and cure of periodic flows at transonic speeds". Proceedings of the 16th Congress of the Int. Council of Aeronautical Science (Jerusalem, Israel), AIAA, Washington D.C., pp. 1522-1530, Aug.-Sept. 1988.
5. Mundell, A. R. G., and Mabey, D. G., "Pressure Fluctuations Caused by Transonic Shock/Boundary Layer Interaction", The Aeronautical Journal, Vol. 90, Aug.-Sept. 1986, pp. 274-281.
6. Seiler F., Srulijes J., George A.: "Vortices and Pressure Waves at Trailing Edges" Proceedings of the 16th International Congress on High Speed Photography and Photonics, Strasbourg, France, 1984.
7. Stanewsky E., Basler D.: Experimental investigation of buffet onset and penetration on a supercritical airfoil at transonic speeds. Aircraft Dynamic Loads Due to Flow Separation, AGARD-CP-483, pp. 4.1-4.11, Sept. 1990.
8. Tijdeman H.: Investigation of transonic flow around oscillating airfoils. National Aerospace Lab. NLR TR 77090, Amsterdam, Oct. 1977.
9. Meyer M.: Grundlagen der Informationstechnik. Vieweg Verlag, 2002.
10. Smith S. W. : The scientist and engineer's guide to digital signal processing. California Technical Publishing, 1997, <http://www.dspguide.com>.
11. Schrufer E.: Signalverarbeitung. Numerische Verarbeitung digitaler Signale. Carl Hanser Verlag, 1990.
12. Olivier, H., Reichel, T., and Zechner, M., "Airfoil Flow Visualization and Pressure Measurements in High-Reynolds-Number Transonic Flow", AIAA Journal, Vol. 41, No. 8, August 2003, pp. 1405-1412.
13. Goepel W., Hesse J., Zemel J. N., (Eds.): Sensors- a comprehensive survey. Band 7. Wiley-VCH Verlagsgesellschaft, Weinheim, 1994
14. Gossweiler C.: Sonden und Messsystem für schnelle aerodynamische Stromungsmessung mit piezoresistiven Druckgebern. Ph.D. Dissertation, ETH Zuerich, 1993.